A receive/transmit calibration technique based on mutual coupling for massive MIMO base stations

Vieira, Joao; Rusek, Fredrik; Tufvesson, Fredrik

Published in:
2016 IEEE 27th Annual International Symposium on Personal, Indoor, and Mobile Radio Communications, PIMRC 2016

DOI:
10.1109/PIMRC.2016.7794649

2016

Document Version:
Peer reviewed version (aka post-print)

A Receive/Transmit Calibration Technique based on Mutual Coupling for Massive MIMO Base Stations

Joao Vieira, Fredrik Rusek, Fredrik Tufvesson
Dept. of Electrical and Information Technology
Lund University, Sweden
firstname.lastname@eit.lth.se

***Abstract*—This paper presents a calibration technique for massive MIMO base stations, where the frequency responses of the transmit and/or receive analog front-ends are individually estimated and compensated for. Calibration is achieved by a first-round of channel sounding between base station antennas, followed by post-processing and a compensation stage. The proposed technique is general in the sense that is does not use external sources, nor internal dedicated circuits for calibration purposes. The only requirement of the technique is that mutual coupling between all pairs of sounded base station antennas exists and is known. Our analysis suggests that mutual coupling can be conveniently used for calibration purposes, and that multipath propagation during calibration is the most prominent source for calibration inaccuracies.**

***Index Terms*—Transceiver calibration, transmit receive estimation, antenna array, mutual coupling, large arrays, massive MIMO.**

I. Introduction

Massive multiple-input multiple output (MIMO) systems have attracted a lot of attention in the wireless research community. In massive MIMO, base stations (BSs) equipped with hundreds of antennas serve a relatively low number of terminals in the same time/frequency resource. This approach holds great promises in terms of energy efficiency, spectral efficiency, etc [1]. However, BSs operating with (very large) antenna arrays usually require some type of calibration to compensate for non-ideal characteristics in the system. These non-idealities are often related to hardware aspects that in theory are assumed ideal for sake of simplicity, but need to be compensated in real systems.

Research efforts to calibrate massive MIMO BSs in order to enable time division duplex (TDD) operation were presented in [2], [3]. These efforts enabled downlink precoding based on non-reciprocal uplink channel estimates. However uplink channel estimates can also be useful for other purposes. For example, the estimates can be used for real time positioning of terminals, for codebook based precoding, or other applications where explicit transmit/receive beamforming are necessary. Indeed, this can only be achieved if the transmit/receive radio-frequency (RF) chains and cables of the BS, are calibrated to yield aligned responses with respect to both phase and magnitude.

The problem setup addressed in this work is as follows. Consider a massive MIMO BS facing an open area, as a typical BS in cellular systems. We envision a calibration procedure that can conveniently be performed on-the-fly, by exchanging signals to-and-from all pairs of BS antennas without the need for external sources nor internal calibration circuits. The received signals are then processed in order to estimate and compensate for the differences between the analog front-ends and cables associated with different antennas. Channels between nearby BS antennas are strongly dominated by mutual coupling effects but nearby reflections can also contribute. No assumptions are made on the array structure nor on the propagation conditions, other than knowing the complex channel gains between all pairs of antennas due to mutual coupling. For a fixed array structure, these quantities can be measured once after array manufacturing and can be considered constant for an arbitrarily long period of time. Note that no user terminals are involved in the calibration process.

For the remainder of this paper, we address calibration as the process of estimating the transmitters/receivers frequency responses, since the compensation stage is straightforward. The measurements in [4] suggest that, with high-end analog components, these estimates are valid for time periods of at least one hour.

A method for transceiver calibration based on signals exchanged among antenna elements of the own array was proposed in [5]. Array shape estimation is performed in a first stage, followed by estimation of the transceiver responses. However, the method proposed in [5] rely on the assumption of spherical wave propagation between antenna elements, which is not suitable for our case due to the strong mutual coupling between BS antennas.

A transceiver calibration method using bi-directional mutual coupling based measurements between adjacent antennas of a 2-dimensional array, was given in [6]. However, all circuitry was made of passive components, e.g. phase shifters and power dividers, yielding a reciprocal channel even including the hardware circuitry. This work generated attention regarding mutual coupling based calibration and spurred many publications, but none fitting the problem setup of this paper. To the best of the authors' knowledge, no calibration work addressing our particular setup is available in the literature.

The remainder of this paper is organized as follows: in Sec. II introduces the signal models. Sec. III presents our proposed estimator and the Cramér-Rao lower bound for the transceiver responses estimates. In Sec. IV the estimator performance is accessed by means of numerical simulations, and finally Sec. V concludes the paper.

II. System models

A. Inter-radio model

Consider an M antenna array where BS transceiver calibration is performed on a flat bandwidth, e.g., a particular subcarrier in an OFDM system. Let for simplicity $x_p = 1$ be the transmitted signal for channel sounding purposes. All antennas are sounded 1-by-1. The vector with the measured forward and reverse channels between radio units n and m with $1 < n < M$, $1 < m < M$ and $m \neq n$ is modeled as

$$\boldsymbol{y}_{n,m} = \begin{bmatrix} y_{n,m} \\ y_{m,n} \end{bmatrix} = h_{n,m} \begin{bmatrix} r_n \, t_m \\ r_m \, t_n \end{bmatrix} + \begin{bmatrix} z_{n,m} \\ z_{m,n} \end{bmatrix}, \quad (1)$$

where the reciprocal propagation channels between antenna elements n and m are described by

$$h_{n,m} = c_{n,m} + \tilde{h}_{n,m}. \quad (2)$$

The term $c_{n,m}$ describes a deterministic and known component due to mutual coupling, which often is stronger for closely spaced antennas. The sum of the remaining multipath contributions are modeled by a zero-mean circularly-symmetric complex Gaussian (ZMCSCG) random variable $\tilde{h}_{n,m}$ with variance σ^2. The non-reciprocal receiver and transmitter frequency responses, that we want to estimate, are modeled by r_m and t_m, respectively, which materially map to the cascade of antenna responses, SMA cables, and all hardware circuitry in the analog front-end stage of the radios. Finally, independent and identically distributed (IID) ZMCSCG noise contributions $z_{n,m}$, each with variance N_0, are assumed.

A few remarks on the modeling assumptions of (1) follow: ***(i)*** The transceiver responses are modeled linearly, although it is well known that front-ends exhibit non-linear behavior in general. The non-linear effects occur mostly due to amplifiers operating close to their saturation point and can be modeled by a sum of one linear and other non-linear terms [7]. Two arguments can be pointed out to justify our pure linearity assumption, the first being that with well behaved amplifiers operating below the compression point, the linear term dominates over the other terms. Secondly, the main goal of the paper is to find a simple way to calibrate the transmitter and receiver responses, and linear modeling simplifies the approach. ***(ii)*** For a fixed antenna array structure, both magnitude and phase of the coupling component $c_{n,m}$ are known. They are can measured once after antenna array manufacturing, and can be considered constant for an arbitrarily long period of time due to the time-invariant properties of the dielectric materials of the array. ***(iii)*** If $\tilde{h}_{n,m}$ is seen as a self-interference channel during calibration[1], then averaging over several realizations of (1) may not necessarily improve the quality of the observations. This is especially true in static scenarios where $\tilde{h}_{n,m}$ has a time-invariant behavior, if $\sigma^2 \gg N_0$. ***(iv)*** Uncorrelated scattering contributions between different antennas are assumed, i.e., $\mathrm{E}\left\{\tilde{h}_{n,m}\tilde{h}^*_{k,p}\right\} = \sigma^2\delta[n-k]\delta[m-p]$. This is a rule-of-thumb in wireless propagation for rich scattering environments for antenna spacings of $\frac{\lambda}{2}$ that we use as an approximation. ***(v)*** For generality purposes, no probabilistic models are assumed for t_m and r_m, i.e., they will be treated as deterministic but unknown parameters for estimation.

[1]This will be seen later in the paper.

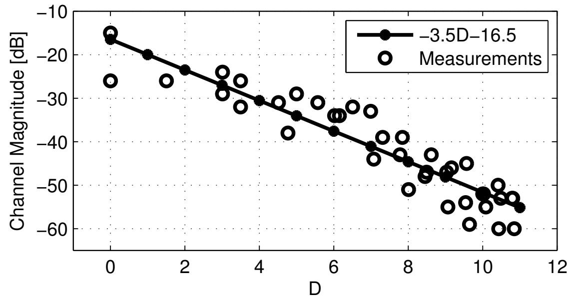

Fig. 1. Measured channel magnitudes (circles) and respective linear regression (solid line). The horizontal axis variable $D = 10\log_{10}\left(\frac{d}{\lambda/2}\right)$ - with d denoting the physical distance between measured antenna pairs - represents the normalized antenna distance in terms of $\lambda/2$ in decibels. For example, the two measurements at $D = 0$ consist of channel magnitudes between two different pairs of adjacent $\lambda/2$ spaced antennas.

B. Modeling the coupling gains between antennas

To allow reproducibility of our simulation results later on, we now give a simple measurement based model for the coupling magnitudes $|c_{m,n}|$. The phases $\angle c_{m,n}$ are drawn from an uniform distribution between $-\pi$ and π. To model $|c_{n,m}|$ as a function of antenna spacing, the channel magnitudes between several pairs of antennas were measured in an anechoic chamber from a 2-dimensional 25x4 dual polarized patch antenna array with $\frac{\lambda}{2}$ spaced elements [4]. The frequency response magnitude over a 20 MHz bandwidth centered at 3.7 GHz - which the array is designed to operate at - was averaged. Fig. 1 shows the measured channel magnitudes as a function of antenna spacing. Different channel magnitudes for equidistant antennas occur due to the relative orientation of the respective antenna pair with respect to the measured E-field polarization. In general, antenna elements placed in the same orientation as the measured E-field polarization couple stronger than others [8]. A linear least square fit has been performed to model the coupling magnitude as a function of antenna distance.

III. Transmitter/Receiver Calibration

A. The Generalized Method of Moments estimator

Introduced originally for statistical inference in econometrics, the Generalized Method of Moments (GMM) is an estimation approach which exploits a particular structure of the signal model, more specifically the *moment conditions* [9]. In our case, a vector of moment conditions $\boldsymbol{g}(\boldsymbol{y}, \boldsymbol{r}, \boldsymbol{t})$ that satisfies

$$\mathrm{E}\{\boldsymbol{g}(\boldsymbol{y}, \boldsymbol{r}, \boldsymbol{t})\} = \mathrm{E}\{\boldsymbol{g}(\boldsymbol{y}, \boldsymbol{\phi})\} = \mathbf{0} \quad (3)$$

is required. In (3), $\boldsymbol{r} = [r_1 \cdots r_M]^T$, $\boldsymbol{t} = [t_1 \cdots t_M]^T$, $\boldsymbol{\phi} = \left[\boldsymbol{t}^T \, \boldsymbol{r}^T\right]^T$, $\mathbf{0}$ is an all zeros column vector, and

$$\boldsymbol{y} = \left[\boldsymbol{y}^T_{1,2} \cdots \boldsymbol{y}^T_{1,M} \; \boldsymbol{y}^T_{2,3} \cdots \boldsymbol{y}^T_{2,M} \cdots \boldsymbol{y}^T_{M-1,M}\right]^T. \quad (4)$$

Noting that all observations in (4) can also be paired as

$$\begin{bmatrix} y_{m,\ell} \\ y_{n,\ell} \end{bmatrix} = \begin{bmatrix} r_m h_{m,\ell} \\ r_n h_{n,\ell} \end{bmatrix} t_\ell + \begin{bmatrix} z_{m,\ell} \\ z_{n,\ell} \end{bmatrix}, \quad (5)$$

with $n \neq \ell \neq m$, inspection indicates a moment condition to be

$$\mathrm{E}\left\{f_{n,m,\ell}\right\} = \mathrm{E}\left\{y_{m,\ell} r_n c_{n,\ell} - y_{n,\ell} r_m c_{m,\ell}\right\} = 0 \;\; \forall\, m, \ell, n. \tag{6}$$

A similar formulation of (5), where instead r_ℓ is the common factor, provides the moment condition

$$\mathrm{E}\left\{d_{n,m,\ell}\right\} = \mathrm{E}\left\{y_{\ell,m} c_{\ell,n} t_n - y_{\ell,n} c_{\ell,m} t_m\right\} = 0 \;\forall\, m, \ell, n. \tag{7}$$

Stacking all useful[2] terms $f_{n,m,\ell}$ in $\boldsymbol{f}\left(\boldsymbol{y}, \boldsymbol{r}\right) \in \mathbb{C}^{M(M-1)/2 \times 1}$, and $d_{n,m,\ell}$ in $\boldsymbol{d}\left(\boldsymbol{y}, \boldsymbol{t}\right) \in \mathbb{C}^{M(M-1)/2 \times 1}$, and denoting $\boldsymbol{g}\left(\boldsymbol{y}, \boldsymbol{\phi}\right) = \left[\boldsymbol{f}\left(\boldsymbol{y}, \boldsymbol{r}\right)^T \boldsymbol{d}\left(\boldsymbol{y}, \boldsymbol{t}\right)^T\right]^T$, the GMM estimator is obtained by solving

$$\hat{\boldsymbol{\phi}} = \arg \min_{\substack{\boldsymbol{\phi} \\ ||\boldsymbol{t}||^2 = M \\ ||\boldsymbol{r}||^2 = M}} \boldsymbol{g}\left(\boldsymbol{y}, \boldsymbol{\phi}\right)^H \hat{\boldsymbol{W}} \boldsymbol{g}\left(\boldsymbol{y}, \boldsymbol{\phi}\right), \tag{8}$$

where $\hat{\boldsymbol{W}}$ is a weighting matrix that generally needs to be optimized. Note the imposed constraint $||\boldsymbol{t}||^2 = ||\boldsymbol{r}||^2 = M$ which avoids the all-zero solution and normalizes the average energy per entry of $\hat{\boldsymbol{\phi}}$ to one. The solution to (8) can be found by standard numerical optimization methods. Newton's algorithm, or any other suitable method, is guaranteed to converge to the global optimum since the problem at hand is quadratic with quadratic constraints. Note that neither $\tilde{h}_{n,\ell}$ nor $\tilde{h}_{m,\ell}$ are included in any of the moment conditions, i.e. only the coupling components are included. Multipath propagation will thus show up as self-interference, as it will be seen later in Sec. IV-B.

We address now the choice of $\hat{\boldsymbol{W}}$. Most of the work within the GMM framework has been done under asymptotic assumptions, i.e., when an infinitely large record of finite signal-to-noise ratio (SNR) observations $\boldsymbol{y}$, or a finite record of infinite SNR observations is at hand. Under such conditions the optimal weighing matrix $\boldsymbol{W}_{\mathrm{opt}}$ has a known form [9]. In our case, only one finite SNR observation is at hand. Depending on the SNR of such observation, the asymptotic regime under which $\boldsymbol{W}_{\mathrm{opt}}$ was derived may not hold. Also, no estimators for $\boldsymbol{W}$ claiming any optimality criteria at the low SNR regime are available in the literature (at least to the best of the authors' knowledge). Claiming no optimality properties on our estimator, we set $\hat{\boldsymbol{W}} = \boldsymbol{I}$ for simplicity, and leave this optimization problem as future work. With $\hat{\boldsymbol{W}} = \boldsymbol{I}$, (8) can be seen as an instance of the Rayleigh quotient problem [10]. Also note that in a calibration setup resembling ours[3], the authors in [3] empirically defined an LS cost function based on their model's inherent structure, not being aware that it corresponds to the particular case of the GMM estimator with $\hat{\boldsymbol{W}} = \boldsymbol{I}$.

[2]There are $M(M-1)$ moment conditions $f_{n,m,\ell}$, however half of them are negative counterparts of the other half and will not contribute for the final cost function.

[3]In their work, calibration between access points of a distributed MIMO system was performed. The estimated parameters were the ratios $\frac{r_m}{t_m}$, and no coupling between antennas was explored. Their moment conditions were also different.

B. Cramér-Rao lower bound for the transmitters/receivers

In this section we compute the Cramér-Rao lower bound (CRLB) [11], a lower bound on the variance of any unbiased estimator, for $\hat{\boldsymbol{\phi}} = \left[\hat{\boldsymbol{t}}^T \hat{\boldsymbol{r}}^T\right]^T$. Assuming[4] $r_1 = t_1 = 1$, we denote the vector of real parameters

$$\boldsymbol{\theta} = [\mathrm{Re}\{t_2\} \;\; \mathrm{Im}\{t_2\} \;\; \mathrm{Re}\{r_2\} \;\; \mathrm{Im}\{r_2\} \;\; \mathrm{Re}\{t_3\} \ldots \mathrm{Im}\{r_M\}]^T, \tag{9}$$

where $\mathrm{Re}\{\}$ and $\mathrm{Im}\{\}$ return real and imaginary part of their arguments, respectively. The CRLB is given by [11]

$$\begin{cases} CRLB(t_m) &= \left[\frac{\boldsymbol{\phi}_0}{\partial \boldsymbol{\theta}} \mathbf{I}^{-1}(\boldsymbol{\theta}) \frac{\boldsymbol{\phi}_0^H}{\partial \boldsymbol{\theta}}\right]_{2m-1, 2m-1} \\ CRLB(r_m) &= \left[\frac{\boldsymbol{\phi}_0}{\partial \boldsymbol{\theta}} \mathbf{I}^{-1}(\boldsymbol{\theta}) \frac{\boldsymbol{\phi}_0^H}{\partial \boldsymbol{\theta}}\right]_{2m, 2m} \end{cases} \tag{10}$$

where $\mathbf{I}(\boldsymbol{\theta}) \in \mathbb{C}^{(2M-2)\times(2M-2)}$ is the Fisher Information matrix of $\boldsymbol{\theta}$, and $\boldsymbol{\phi}_0 = [t_2 \; r_2 \; t_3 \; r_3 \; \cdots \; t_M \; r_M]^T$. Before computing $\mathbf{I}(\boldsymbol{\theta})$, note that the mean of (1) is given by

$$\boldsymbol{\mu}_{n,m} = \mathrm{E}\left\{\boldsymbol{y}_{n,m}\right\} = c_{n,m} \left[r_n t_m \;\; r_m t_n\right]^T, \tag{11}$$

and the covariance matrix of (1) is given by

$$\begin{aligned} \boldsymbol{\Sigma}_{n,m} &= \mathrm{Var}\left\{\boldsymbol{y}_{n,m} \boldsymbol{y}_{n,m}^H\right\} \\ &= \begin{bmatrix} |r_n|^2 |t_m|^2 \sigma^2 + N_0 & r_n t_m r_m^* t_n^* \sigma^2 \\ r_m t_n r_n^* t_m^* \sigma^2 & |r_m|^2 |t_n|^2 \sigma^2 + N_0 \end{bmatrix}. \end{aligned} \tag{12}$$

We can observe that the likelihood function for (4) is a multivariate Gaussian PDF, i.e., $p(\boldsymbol{y}|\boldsymbol{\theta}) \sim \mathcal{CN}(\boldsymbol{\mu}, \boldsymbol{\Sigma})$, with mean $\boldsymbol{\mu} = \left[\boldsymbol{\mu}_{1,2}^T \cdots \boldsymbol{\mu}_{1,M}^T \boldsymbol{\mu}_{2,3}^T \cdots \boldsymbol{\mu}_{2,M}^T \cdots \boldsymbol{\mu}_{M-1,M}^T\right]^T$ and block diagonal covariance

$$\boldsymbol{\Sigma} = \mathrm{diag}\left\{\boldsymbol{\Sigma}_{1,2}, \cdots, \boldsymbol{\Sigma}_{1,M}, \boldsymbol{\Sigma}_{2,3}, \cdots, \boldsymbol{\Sigma}_{2,M}, \cdots, \boldsymbol{\Sigma}_{M-1,M}\right\}. \tag{13}$$

For such likelihood form, the Fisher Information matrix entry at the ith row and jth column is given by

$$\begin{aligned} \left[\mathbf{I}(\boldsymbol{\theta})\right]_{i,j} = &\; \mathrm{Tr}\left\{\boldsymbol{\Sigma}^{-1} \frac{\partial \boldsymbol{\Sigma}}{\partial \theta_i} \boldsymbol{\Sigma}^{-1} \frac{\partial \boldsymbol{\Sigma}}{\partial \theta_j}\right\} \\ &+ 2 \;\; \mathrm{Re}\left\{\frac{\partial \boldsymbol{\mu}^H}{\partial \theta_i} \boldsymbol{\Sigma}^{-1} \frac{\partial \boldsymbol{\mu}}{\partial \theta_j}\right\}. \end{aligned} \tag{14}$$

Note that i and j can also be expressed as $i = 4(m-1) + K_m$ and $j = 4(n-1) + K_n$, with $1 < K_m < 4$ and $1 < K_n < 4$.

Due to the symmetric property of $\mathbf{I}(\boldsymbol{\theta})$ and thus assuming $j \geq i$, (14) can be written as

$$\left[\mathbf{I}(\boldsymbol{\theta})\right]_{i,j} = \begin{cases} A_1 + A_2, & m \neq n \\ B_1 + B_2, & m = n \end{cases} \tag{15}$$

[4]See Sec. III-C for justification.

with

$$A_1 = \operatorname{Tr}\left\{\mathbf{\Sigma}_{m,n}^{-1}\frac{\partial\mathbf{\Sigma}_{m,n}}{\partial\theta_i}\mathbf{\Sigma}_{m,n}^{-1}\frac{\partial\mathbf{\Sigma}_{m,n}}{\partial\theta_j}\right\},$$

$$B_1 = \sum_{\ell>m}^{M}\operatorname{Tr}\left\{\mathbf{\Sigma}_{m,\ell}^{-1}\frac{\partial\mathbf{\Sigma}_{m,\ell}}{\partial\theta_i}\mathbf{\Sigma}_{m,\ell}^{-1}\frac{\partial\mathbf{\Sigma}_{m,\ell}}{\partial\theta_j}\right\} + \sum_{\ell=1}^{n}\operatorname{Tr}\left\{\mathbf{\Sigma}_{\ell,m}^{-1}\frac{\partial\mathbf{\Sigma}_{\ell,m}}{\partial\theta_i}\mathbf{\Sigma}_{\ell,m}^{-1}\frac{\partial\mathbf{\Sigma}_{\ell,m}}{\partial\theta_j}\right\},$$

$$A_2 = 2\operatorname{Re}\left\{\frac{\partial\boldsymbol{\mu}_{m,n}^H}{\partial\theta_i}\mathbf{\Sigma}_{m,n}^{-1}\frac{\partial\boldsymbol{\mu}_{m,n}}{\partial\theta_j}\right\},$$

$$B_2 = 2\operatorname{Re}\left\{\sum_{\ell>m}^{M}\frac{\partial\boldsymbol{\mu}_{m,\ell}^H}{\partial\theta_i}\mathbf{\Sigma}_{m,\ell}^{-1}\frac{\partial\boldsymbol{\mu}_{m,\ell}}{\partial\theta_j}\right\} + 2\operatorname{Re}\left\{\sum_{\ell=1}^{m}\frac{\partial\boldsymbol{\mu}_{\ell,m}^H}{\partial\theta_i}\mathbf{\Sigma}_{\ell,m}^{-1}\frac{\partial\boldsymbol{\mu}_{\ell,m}}{\partial\theta_j}\right\}.$$

An example of a derivative of (12) with respect to an entry of $\boldsymbol{\theta}$ is given in the appendix.

Note the general block diagonal structure of $\frac{\partial\mathbf{\Sigma}}{\partial\theta_i}$, e.g., for $\frac{\partial\mathbf{\Sigma}}{\partial\theta_7}$ (where $m = 2$ and $K_m = 3$) we have

$$\frac{\partial\mathbf{\Sigma}}{\partial\theta_7} = \operatorname{diag}\left\{\frac{\partial\mathbf{\Sigma}_{1,2}}{\partial\theta_7}, \boldsymbol{\emptyset}, \cdots, \boldsymbol{\emptyset}, \frac{\partial\mathbf{\Sigma}_{2,3}}{\partial\theta_7}, \cdots, \frac{\partial\mathbf{\Sigma}_{2,M}}{\partial\theta_7}, \boldsymbol{\emptyset}, \cdots\right\} \tag{16}$$

where $\boldsymbol{\emptyset}$ is an all zero matrix. If $m \neq n$, there is only one matrix entry where the two block diagonal matrices $\frac{\partial\mathbf{\Sigma}}{\partial\theta_i}$ and $\frac{\partial\mathbf{\Sigma}}{\partial\theta_i}$ are non-zero. If $m = n$, then M of such matrix entries are shared which explains the summations in A_2 and B_2. To finalize, note that both N_0 and σ^2 were assumed to be known in the CRLB computation.

C. A Reference Element for Calibration

The CRLB computations for $\hat{t}_m$ and $\hat{r}_m$ made use of the concept of a reference antenna element for calibration purposes, see [2]. That is, since calibration can be performed up to a common complex factor among the transceivers, a convenient approach is to assume $r_1 = t_1 = 1$ where such transceiver is considered a reference[5]. The CRLB for the remaining elements are calculated accordingly. This ensures invertibility for the Fisher Information matrix. However, note that setting $r_1 = t_1 = 1$ needs not to be strictly met to derive an estimator, as done in Sec. III-A.

IV. Performance Assessment

A. Simulation Setup

The main focus of our analysis contrasts the GMM estimator mean square error (MSE) against the CRLB. We define the following MSE metric for the GMM estimator performance:

$$\begin{aligned} MSE(r_m) &= \left[\ \mathrm{E}\left\{|\boldsymbol{r} - \hat{\boldsymbol{r}}/\hat{r}_1|^2\right\}\ \right]_m \\ MSE(t_m) &= \left[\ \mathrm{E}\left\{|\boldsymbol{t} - \hat{\boldsymbol{t}}/\hat{t}_1|^2\right\}\ \right]_m. \end{aligned} \tag{17}$$

[5]More generally, one can assume $r_m = q_1$ and $t_m = q_2$ with $\mathbf{0} \neq [q_1\ q_2]^T \in \mathbb{C}^{2\times1}$.

This MSE definition is coherent with the reference element concept used in the CRLB calculations. Moreover, our numerical simulations for the GMM estimator and CRLB computations were all performed with $r_m = t_m = 1\ \forall\ m$. The constraint in (8), namely $||\boldsymbol{t}||^2 = ||\boldsymbol{r}||^2 = M$, ensures that

$$\hat{\boldsymbol{\phi}}_0 \xrightarrow{p} \boldsymbol{\phi}_0 \ \text{ as } \begin{cases} N_0 \to 0 \\ \sigma^2 \to 0 \end{cases} \tag{18}$$

due to the asymptotically unbiasedness property of the GMM estimator [9]. The notation $\xrightarrow{p}$ denotes convergence in probability. The unbiasedness property in (18), and the MSE definition in (17), allow a coherent comparison between the estimator MSE and the CRLB. Also, having $r_m = t_m = 1$ makes MSE $= 0$ dB a reference point in the analysis.

Naturally, we select the reference element as one of the most central antenna elements of the 2-dimensional array. In average, this choice yields the strongest coupling channels to all other antenna elements of the array.

We limit our analysis to two extreme cases, namely, calibration of a transceiver which is associated to an adjacent (or neighbor) antenna element to the reference element, and the case of calibration of a transceiver that is associated with one of the antennas at the four corners (edges) of the 2D array.

Note that all upcoming results, and evaluated range of N_0 and σ^2, should be considered together with the derived coupling model in Fig. 1 where the strongest coupling channel, i.e. neighbor channel, yields a -16.5 dB gain.

B. Results and Analysis

The symmetry of the model in (1) for r_m and t_m together with the simulations settings adopted, makes the statistical performance of $\hat{r}_m$ similar to $\hat{t}_m$. Thus, our analysis holds for both cases.

Fig. 2 shows the CRLB for the transceiver associated with a neighbor antenna with respect to the reference. Overall, this lower bound of the variance decreases as M increases due to the increasing number of signal alternatives available to estimate the same parameter. At low enough N_0, the CRLB flattens out which happens due to the self-interference term $\tilde{h}_{m,n}$.

The CRLB for the edge antenna transceivers is shown in Fig. 3. An increase of M also decreases the CRLB as in the neighbor case. An interesting fact, since, although a larger signal set is available for estimation purposes, the distance (and hence the path loss) with respect to the reference element also increases. Compared to the neighbor case, a performance degradation of up to 4 dB is to be expected, as can be seen in Fig. 6 in Appendix B.

Fig. 4 and 5 show the MSE performance of the GMM estimator, and contrast this with the CRLB for $M = 100$ antenna elements. For the neighbor antenna case, performance very close to the theoretical optimum is achieved for some parameter regions, e.g. $N_0 \approx -35$ dB and $\sigma^2 = -50$ dB for $M = 36$ and $M = 100$.

Since we set $t_m = r_m = 1\ \forall m$ in our simulations, increasing N_0 or σ^2 by the same amount is equally degrading for the performance of our estimator. For example when

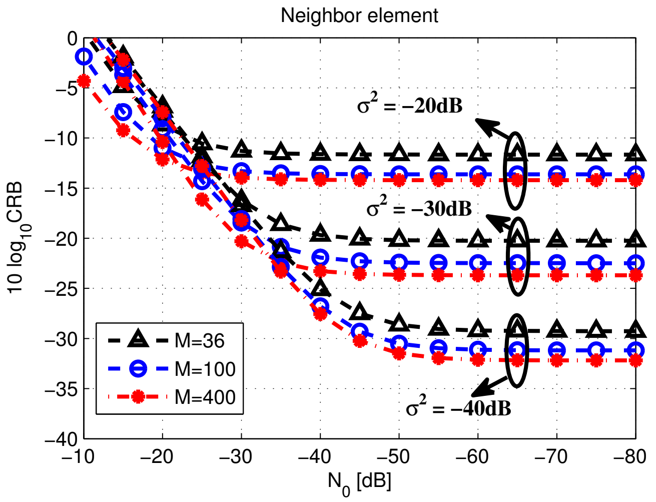

Fig. 2. CRLB vs N_0 for the neighbor antenna element, for different number of base station antennas M, and parameter of the Rayleigh channel σ.

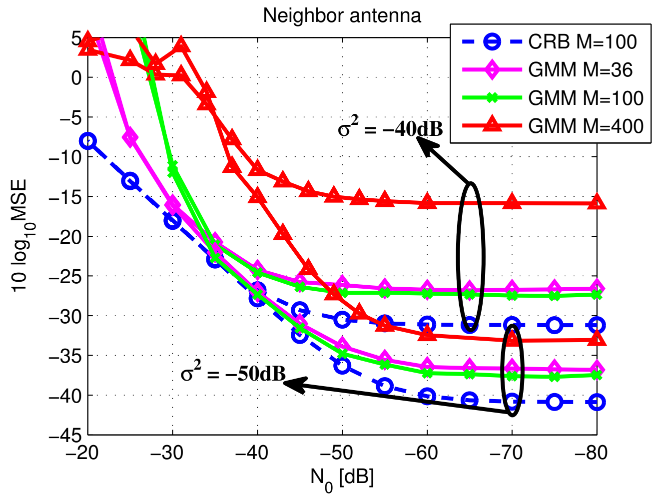

Fig. 4. MSE of the GMM estimator vs N_0 for the neighbor antenna element, for different number of base station antennas M, and parameter of the Rayleigh channel σ.

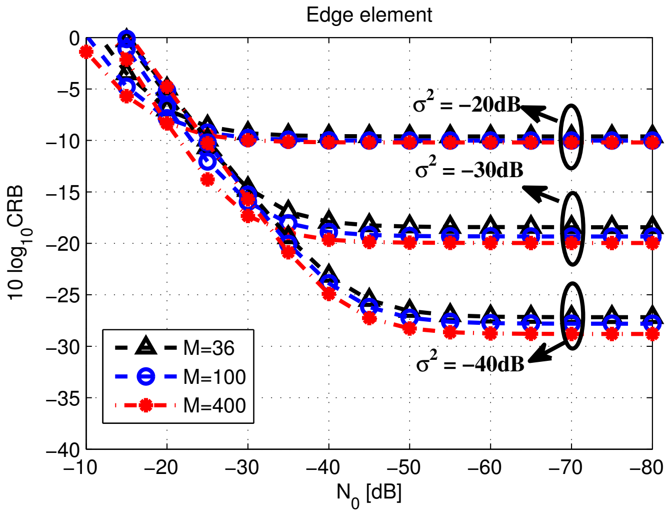

Fig. 3. CRLB vs N_0 for the edge antenna element, for different number of base station antennas M, and parameter of the Rayleigh channel σ.

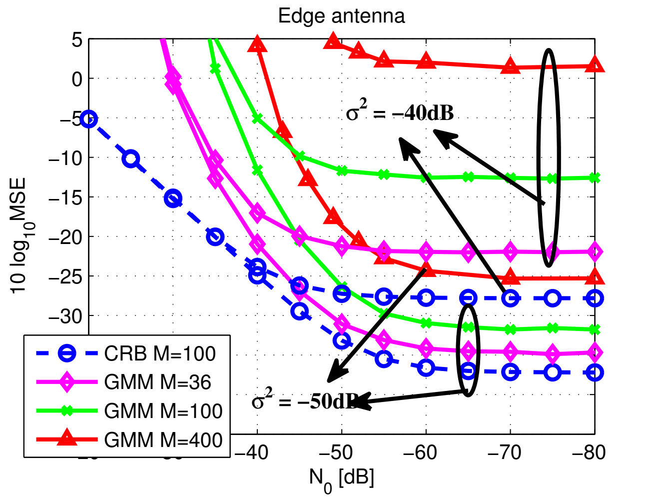

Fig. 5. MSE of the GMM estimator vs N_0 for the edge antenna element, for different number of base station antennas M, and parameter of the Rayleigh channel σ.

$M = 400$ in Fig. 4, an MSE of -27 dB is obtained for $\sigma^2 = N_0 = -50$ dB, and increasing σ^2 or N_0 by 10 dB results in an MSE of -15 dB. It is worthwhile mentioning that in a practical scenario, increasing the transmit power beyond a certain level is not beneficial to improve the quality of the observations, since $\tilde{h}_{n,m}$ multiplies the transmit signal. This aspect together with a possible time-invariant behavior of $\tilde{h}_{n,m}$, which results in no quality improvements by averaging, makes multipath propagation a prominent source for calibration inaccuracies.

Overall, GMM calibration for neighboring antennas is more accurate than for edge antennas, as one would expect. However some calibration cases indicate that performance degradation seems to always increase with M. This is particularly true for the edge antenna element, contrarily with one would expect simple by analyzing their CRLBs for different M. The sub-optimality of our estimator may justify this behavior.

V. Conclusions

In this paper, a transceiver calibration technique using mutual coupling between antenna elements of a massive MIMO base station was proposed. For a 2-dimensional antenna array of a given size, transceivers associated with antennas at the edge of the array are the hardest to calibrate. Moreover, the results from our proposed estimator indicate that the calibration error associated with these transceivers grows for arrays with increasing number of antennas. This implies that in practice, stricter calibration requirements are needed to calibrate bigger arrays, while still maintaining the same error criterion. This is however contrary to what the CRLB indicates.

Overall, the proposed calibration method does not suffer from convergence problems, and it is of practical use, given that the mutual coupling gains between BS antennas are known, and multipath contributions during calibration are small compared to mutual coupling effects.

ACKNOWLEDGMENTS

The research leading to these results has been funded by grants from the Swedish foundation for strategic research SSF, the Swedish research council, the Excellence center at Linkoping - Lund in Information Technology, and the European Union Seventh Framework Programme (FP7/2007-2013) under grant agreement n 619086 (MAMMOET).

VI. APPENDIX A

Fig. 6 shows the difference between the CRLB of a transceiver estimate associated with edge antennas, and transceiver estimate associated with neighbor antennas to the reference antenna.

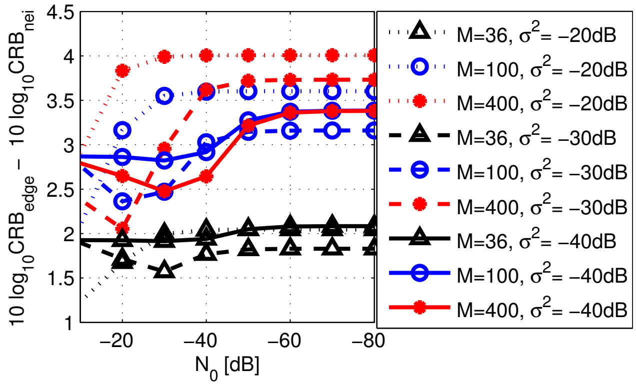

Fig. 6. Difference between the CRLB of a transceiver estimate associated with edge antennas, and transceiver estimate associated with neighbor antennas to the reference antenna, for different number of BS antennas M, and squared parameter of the Rayleigh channel σ^2.

VII. APPENDIX B

An example of a derivative of (12) with respect to an entry of $\boldsymbol{\theta}$, namely $\theta_{4(k-1)+K_m}$ with $K_m = 2$ given by

$$\frac{\partial \Sigma_{i,j}}{\partial \operatorname{Im}\{t_k\}} = \begin{cases} \begin{bmatrix} 0 & -jr_i t_j r_j^* \sigma^2 \\ jr_i^* t_j^* r_j \sigma^2 & 2\operatorname{Im}\{t_i\}|r_j|^2\sigma^2 \end{bmatrix}, & k = i \\ \begin{bmatrix} 2\operatorname{Im}\{t_j\}|r_i|^2\sigma^2 & jr_i r_j^* t_i^* \sigma^2 \\ -jr_j t_i r_i^* \sigma^2 & 0 \end{bmatrix}, & k = j \\ \varnothing, & \text{otherwise.} \end{cases}$$

REFERENCES

[1] E. Larsson, O. Edfors, F. Tufvesson, and T. Marzetta, “Massive MIMO for next generation wireless systems,” *Communications Magazine, IEEE*, vol. 52, no. 2, pp. 186–195, February 2014.

[2] C. Shepard, H. Yu, N. Anand, E. Li, T. Marzetta, R. Yang, and L. Zhong, “Argos: Practical many-antenna base stations,” in *Proceedings of the 18th Annual International Conference on Mobile Computing and Networking*, ser. Mobicom ’12. New York, NY, USA: ACM, 2012, pp. 53–64.

[3] R. Rogalin, O. Bursalioglu, H. Papadopoulos, G. Caire, A. Molisch, A. Michaloliakos, V. Balan, and K. Psounis, “Scalable synchronization and reciprocity calibration for distributed multiuser MIMO,” *Wireless Communications, IEEE Transactions on*, vol. 13, no. 4, pp. 1815–1831, April 2014.

[4] J. Vieira, S. Malkowsky, K. Nieman, Z. Miers, N. Kundargi, L. Liu, I. Wong, V. Öwall, O. Edfors and F. Tufvesson, “A flexible 100-antenna testbed for Massive MIMO,” in *IEEE GLOBECOM 2014 Workshop on Massive MIMO: from theory to practice, 2014-12-08*. IEEE, 2014.

[5] M. Willerton, “Array auto-calibration,” Ph.D. dissertation, Imperial College London, U.K., 2013.

[6] H. Aumann, A. Fenn, and F. Willwerth, “Phased array antenna calibration and pattern prediction using mutual coupling measurements,” *Antennas and Propagation, IEEE Transactions on*, vol. 37, no. 7, pp. 844–850, Jul 1989.

[7] F. Ghannouchi and O. Hammi, “Behavioral modeling and predistortion,” *Microwave Magazine, IEEE*, vol. 10, no. 7, pp. 52–64, Dec 2009.

[8] R. Jedlicka, M. Poe, and K. Carver, “Measured mutual coupling between microstrip antennas,” *Antennas and Propagation, IEEE Transactions on*, vol. 29, no. 1, pp. 147–149, Jan 1981.

[9] A. Hall, *Generalized Method of Moments*, ser. Advanced Texts in Econometrics. OUP Oxford, 2004.

[10] P. Lancaster and M. Tismenetsky, *The Theory of Matrices: With Applications*, ser. Computer Science and Scientific Computing Series. Academic Press, 1985.

[11] S. M. Kay, *Fundamentals of Statistical Signal Processing: Estimation Theory*. Upper Saddle River, NJ, USA: Prentice-Hall, Inc., 1993.